Supporting Information

Owens et al. 10.1073/pnas.1305304110

SI Materials and Methods

We present results from four localities in Europe spanning intervals before, during, and after Oceanic Anoxic Event 2 (OAE 2). The sample locations were selected with an eye toward sites that had direct connection to the open ocean and a spatial distribution that encompasses multiple marine basins (Fig. 1). All sample sites have been previously documented to record the OAE 2 interval by means of biostratigraphy, chemostratigraphy (Sr-and C isotopes), or a combination of both (1–5). A comprehensive discussion of the sedimentology, age relationships, and tectonic settings of the sampled localities is already available (2, 5–7). All of the sections are dominated by carbonate lithologies with abundant microfossils, along with some macrofossils, and are characterized by low organic carbon contents (2, 5–7), with one exception. The section at South Ferriby contains a 10-cm-thick organic-rich interval deposited during OAE 2 (2, 4), which was avoided for carbonate-associated sulfate (CAS) analysis. We chose these carbonate sites because they can capture evolving global seawater chemistry, which tracks ocean-scale redox processes. Importantly, because organic-lean sites typically provide lithologic uniformity before, during, and after the OAE, they potentially represent the best isotopic archives of global marine conditions. Briefly, three of the four localities (Eastbourne cliff section, South Ferriby Quarry, and the Trunch borehole: all United Kingdom) illustrate poorly lithified pelagic foraminiferal–nannofossil-rich chalk facies with similar diagenetic histories and consistently good carbonate preservation. The fourth sample site, Raia del Pedale, is a well-lithified platform-carbonate section in southern Italy, rich in rudist fragments and benthic foraminifera and formerly located on the margin of the Tethys Ocean (Fig. 1). Fig. 2 shows lithostratigraphic sections and carbon isotopes for South Ferriby from Jenkyns et al. (4), stratigraphy for Trunch borehole from Jarvis et al. (3) (note $\delta^{13}C$ from bulk pelagic carbonate), and stratigraphic data and carbon isotopes for the Eastbourne section from Tsikos et al. (1).

All samples analyzed for the $\delta^{34}S_{CAS}$ were dominated by high carbonate contents (60–80 wt%). We followed a standard procedure extracting CAS from the carbonate-rich samples (8, 9). Briefly, the samples were trimmed to eliminate weathered surfaces, including surficial Fe oxidation. Then, 10–20 g of powdered sample were treated with NaCl and NaOCl solutions and rinsed with multiple deionized rinses to prevent the incorporation of any non-CAS sulfur-bearing phases. The samples were then dissolved using 4 M HCl and vacuum-filtered less than 1 h later to minimize the pyrite oxidation, which was further limited in the samples by low pyrite and ferric iron concentrations. A $BaCl_2$ solution was added to precipitate sulfate as $BaSO_4$.

The precipitated and homogenized $BaSO_4$ from each sample was loaded into tin capsules with excess V_2O_5 and analyzed for its $^{34}S/^{32}S$ ratio at the University of California, Riverside. Sulfur-isotope ratios were measured using a Thermo Delta V gas-source isotope-ratio mass spectrometer coupled to a Costech 4010 elemental combustion system for on-line sample combustion and analysis. All sulfur-isotope compositions are reported in standard delta notation as per mil (‰) deviation relative to Vienna Canyon Diablo Troilite and were corrected to a suite of international reference materials using a linear regression (e.g., refs. 8, 9) based on replicate analyses of international standards [International Atomic Energy Agency (IAEA) SO-5 [0.49], IAEA SO-6 [−34.05], and NBS 127 [21.1]] agreed to within 0.2‰ of their published values.

C and S Modeling. The values used in the coupled carbon and sulfur model were based on the combination of available geochemical data and on the sensitivity tests (Fig. 4) to help constrain unknown parameters for the sulfur cycle. As previously stated, there are several possibilities to replicate the observed trends by mixing and matching unconstrained parameters, but we have attempted to bracket a few of these factors using data in combination with estimates for these values in the modern cycles. For instance, the $\Delta^{34}S$ used in the model during non-OAE intervals is close to the modern value and was necessary to achieve steady state with the inputs, whereas the ΔS during the OAE itself was chosen based on the known starting sulfate value (∼+20‰; ref. 10) and an average pyrite value of −20‰ [the average pyrite value during the OAE based on the available data is ∼−30‰ (11–14), but this is exclusively from euxinic settings and we assume a global average closer to −20‰], which provides a $\Delta^{34}S$ of −40‰. Consequently, the $\Delta^{34}S$ is transiently shifted in the model from −30‰ to −40‰ and back to −30‰ for the intervals prior to, during, and after the OAE, respectively. The starting sulfate concentration was based on the length of time it takes for the S-isotope profile of the Raia del Pedale section to indicate recovery to the pre-OAE baseline and seems to fit best with values between 5 and 9 mM and thus we used the average of 7 mM. The values for continental weathering were held constant with the exception of the enhanced weathering scenario (discussed previously), which would only dampen the positive excursion. Therefore, the only parameter to further adjust is the amount of pyrite burial, which can have dramatic effects on the magnitude of the excursion.

To model the carbon isotope excursion in the modeling exercises, all parameters are held constant in the carbon cycle and the burial of organic carbon is increased to 1.6× the pre-excursion rate. For the sulfur cycle portion of the model, we used the values discussed above and increased the pyrite burial rate to 2× the starting rate because it best replicated a 5–6‰ excursion; however, adjusting this value does not affect the offset between the carbon- and sulfur-isotope excursions. Replicating this offset requires a waning of the carbon and sulfur burial rates (shown in Fig. S1). The longer the transient decay back to the pre-OAE baseline burial rates, the larger the offset because of the differences of sizes of dissolved inorganic carbon (DIC) and sulfate reservoirs and relative magnitude of the fluxes in the cycles compared with this reservoir size. Consequently the peak carbon-isotope values occur closer to the time of maximum organic-carbon burial (i.e., near the end of the OAE), but the sulfur excursion continues to rise until the return to normal pyrite burial as seen in Fig. S1.

Eastbourne Sulfur Geochemical Preservation. The $\delta^{34}S_{CAS}$ at this site shows several negative shifts during the first half of the OAE, although the overall trend of the data shows progressively more positive values. Eastbourne shows small negative excursions within the OAE, although the Raia del Pedale section seems to indicate similar features. These negative excursions in the Eastbourne section seem to be correlated with the most positive $\delta^{13}C_{carb}$ values before the slight decreases in carbon-isotope values. It is difficult to pinpoint the exact origin of the negative excursions at Eastbourne but there are three possibilities to explain the observed phenomena: (*i*) later pyrite oxidation skewing the primary CAS signal, (*ii*) enhanced delivery of sulfate, or (*iii*) a paleoceanographic circulation change.

A concern for the validity of the data for CAS has been the oxidation of pyrite either during the burial of the rock, outcrop weathering, or during the chemical extraction of CAS (15, 16). Due to the slight decrease in carbonate concentration leading into the OAE (on average 83 wt% in OAE chalk sediment and ~91 wt% in non-OAE chalk sediment) this could be a concern. With this in mind, we measured the amount of pyrite in most samples postfiltration of the CAS dissolution step and performed a standard chromium chloride extraction (17). The low amounts of pyrite measured for all sections (Fig. S2), with Eastbourne having the highest values but relatively low compared with previously published CAS data sets (8, 9, 18–21), suggest this effect played a limited role during the extraction procedure. In addition, cross-plots of sulfate isotopes and sulfate concentrations against the pyrite concentration show no trends for individual sections (Fig. S2) or all samples combined. Also, CAS isotope vs. pyrite concentration for Eastbourne shows no linear correlation or obvious trends. Linear correlations with pyrite would imply a mixed signal of primary CAS and pyrite-contaminated sulfate (9, 15, 16); therefore, we believe this signal is a primary $\delta^{34}S_{CAS}$ signal.

Geochemical proxies suggest there was an increase of continental weathering during the OAE (22–24) or increased volcanic activity (13), phenomena which could have delivered isotopically depleted sulfur to the marine reservoir. This model seems unlikely, because a simple mass-balance calculation would suggest that a massive delivery of sulfate would have had to enter the system to account for the isotopic shift. Furthermore, there is no evidence for increased marine sulfate concentrations during the OAE that would necessarily have affected all localities equally.

The third possibility for the $\delta^{34}S_{CAS}$ record that the negative excursions observed at Eastbourne are changes in the paleoceanographic circulation patterns due to climatic processes. There is mounting evidence for a cooling episode during the early part of the OAE, not only due to silicate weathering but also to the global burial of organic carbon, thus decreasing atmospheric CO_2 (25–28). The fall in temperature is documented by the paleotemperature proxy tetraether index $(TEX)_{86}$ (29, 30) in the Northern proto-Atlantic and by invasion of boreal faunas (the so-called "Plenus Cold Event") in the north European Chalk Sea (31), both accompanied by excursions in Nd-isotope ratios, suggesting introduction of watermasses of possible Arctic derivation (32–34). In the proto-Atlantic region and the Western Interior Seaway, the invasion of cooler, more oxygenated waters during the same time interval was characterized by population of the seafloor by benthic foraminifera: the so-called "Benthic Oxic Event" (35, 36). Such oxygenated waters as these would have oxidized subseafloor surficial pyrite and introduced isotopically depleted sulfate into the water column and thus lowered the S-isotope composition of ambient seawater.

1. Tsikos H, et al. (2004) Carbon-isotope stratigraphy recorded by the Cenomanian–Turonian Oceanic Anoxic Event: Correlation and implications based on three key localities. *J Geol Soc London* 161:711–719.
2. Schlanger SO, Arthur MA, Jenkyns HC, Scholle PA (1987) The Cenomanian-Turonian Oceanic Anoxic Event, I. Stratigraphy and distribution of organic carbon-rich beds and the marine δ13C excursion. *Marine Petroleum Source Rocks,* eds Brooks J, Fleet AJ (Geological Society, London), Special Publications, Vol 26, pp 371–399.
3. Jarvis I, Gale AS, Jenkyns HC, Pearce MA (2006) Secular variation in Late Cretaceous carbon isotopes: A new Campanian (99.6-70.6 Ma). *Geol Mag* 143:561–608.
4. Jenkyns HC, Matthews A, Tsikos H, Erel Y (2007) Nitrate reduction, sulfate reduction, and sedimentary iron isotope evolution during the Cenomanian-Turonian oceanic anoxic event. *Paleoceanography* 22:PA3208.
5. Parente M, et al. (2008) Stepwise extinction of larger foraminifers at the Cenomanian-Turonian boundary: A shallow-water perspective on nutrient fluctuations during Oceanic Anoxic Event 2 (Bonarelli Event). *Geology* 36:715–718.
6. Wood CJ, Morter AA, Gallois RW (1994) Upper Cretaceous stratigraphy of the Trunch borehole. *Geology of the Country around Great Yarmouth Memoir for 1:50,000 Sheet 162 (England and Wales) with an Appendix on the Trunch Borehole by Wood and Morter*, eds Arthurton RS, Booth SJ, Morigi AN, Abbott MAW, Wood CJ (HMSO, London), pp 105–110.
7. Gale AS, Jenkyns HC, Kennedy WJ, Corfield RM (1993) Chemostratigraphy versus biostratigraphy: Data from around the Cenomanian-Turonian boundary. *J Geol Soc London* 150:29–32.
8. Gill BC, Lyons TW, Jenkyns HC (2011) A global perturbation to the sulfur cycle during the Toarcian Oceanic Anoxic Event. *Earth Planet Sci Lett* 312:484–496.
9. Gill BC, et al. (2011) Geochemical evidence for widespread euxinia in the later Cambrian ocean. *Nature* 469(7328):80–83.
10. Paytan A, Kastner M, Campbell D, Thiemens MH (2004) Seawater sulfur isotope fluctuations in the Cretaceous. *Science* 304(5677):1663–1665.
11. van Bentum EC, et al. (2009) Reconstruction of water column anoxia in the equatorial Atlantic during the Cenomania-Turonian oceanic anoxic event using biomarker and trace metal proxies. *Palaeogeogr Palaeoclimatol Palaeoecol* 280:489–498.
12. Gautier DL (1987) Isotopic composition of pyrite: Relationship to organic matter type and iron availability in some North American Cretaceous shales. *Chem Geol Isot Geosci Sect* 65:293–303.
13. Adams DD, Hurtgen MT, Sageman BB (2010) Volcanic triggering of a biogeochemical cascade during Oceanic Anoxic Event 2. *Nat Geosci* 3:201–204.
14. Böttcher ME, Hetzel A, Brumsack HJ, Schipper A (2006) Sulfur–iron–carbon geochemistry in sediments of the Demerara Rise. *Proceedings of the Ocean Drilling Program. Scientific Results*, eds Mosher, DC, Erbacher, J, Malone, MJ (Ocean Drilling Program, College Station, TX), Vol 207, pp 1–23.
15. Marenco PJ, Corsetti FA, Kaufman AJ, Bottjer DJ (2008) Environmental and diagenetic variations in carbonate associated sulfate: An investigation of CAS in the Lower Triassic of the western USA. *Geochim Cosmochim Acta* 72:1570–1582.
16. Mazumdar A, Goldberg T, Strauss H (2008) Abiotic oxidation of pyrite by Fe(III) in acidic media and its implications for sulfur isotope measurements of lattice-bound sulfate in sediments. *Chem Geol* 253:30–37.
17. Canfield DE, et al. (1986) The use of chromium reduction in the analysis of reduced inorganic sulfur in sediments and shales. *Chem Geol* 54:149–155.
18. Fike DA, Grotzinger JP, Pratt LM, Summons RE (2006) Oxidation of the Ediacaran ocean. *Nature* 444:744–747.
19. Fike DA, Grotzinger JP (2008) A paired sulfate-pyrite $\delta^{34}S$ approach to understanding the evolution of the Ediacaran-Cambrian sulfur cycle. *Geochim Cosmochim Acta* 72:2636–2648.
20. Wotte T, Strauss H, Fugmann A, Garbe-Schönberg D (2012) Paired $\delta^{34}S$ data from carbonate-associated sulfate and chromium-reducible sulfur across the traditional Lower–Middle Cambrian boundary of W-Gondwana. *Geochim Cosmochim Acta* 85:228–253.
21. Loyd SJ, et al. (2012) Sustained low marine sulfate concentrations from the Neoproterozoic to the Cambrian: Insights from carbonates of northwestern Mexico and eastern California. *Earth Planet Sci Lett* 339-40:79–94.
22. Blättler CL, Jenkyns HC, Reynard LM, Henderson GM (2011) Significant increases in global weathering during Oceanic Anoxic Events 1a and 2 indicated by calcium isotopes. *Earth Planet Sci Lett* 309:77–88.
23. Frijia G, Parente M (2008) Strontium isotope stratigraphy in the upper Cenomanian shallow-water carbonates of the southern Apennines: Short-term perturbations of marine $^{87}Sr/^{86}Sr$ during the oceanic anoxic event 2. *Palaeogeogr Palaeoclimatol Palaeoecol* 261:15–29.
24. Pogge von Strandmann PAE, Jenkyns HC, Woodfine RG (2013) Lithium isotope evidence for enhanced weathering during Oceanic Anoxic Event 2. *Nat Geosci* 6:668–672.
25. van Bentum EC, Reichart G-J, Forster A, Sinninghe Damsté JS (2012) Latitudinal differences in the amplitude of the OAE-2 carbon isotopic. *Biogeosciences* 9:717–731.
26. Jarvis I, et al. (2011) Black shale deposition, atmospheric CO2 drawdown, and cooling during the Cenomanian-Turonian Oceanic Anoxic Event. *Paleoceanography* 26:PA3201.
27. Barclay RS, McElwain JC, Sageman BB (2010) Carbon sequestration activated by a volcanic CO_2 pulse during Ocean Anoxic Event 2. *Nat Geosci* 3:205–208.
28. Arthur MA, Dean WE, Pratt LM (1988) Geochemical and climatic effects of increased marine organic carbon burial at the Cenomanian/Turonian boundary. *Nature* 335:714–717.
29. Forster A, et al. (2007) Tropical warming and intermittent cooling during the Cenomanian/Turonian oceanic anoxic event 2: Sea surface temperature records from the equatorial Atlantic. *Paleoceanography* 22:PA1219.
30. Sinninghe Damsté JS, et al. (2010) A CO_2 decrease-driven cooling and increased latitudinal temperature gradient during the mid-Cretaceous Oceanic Anoxic Event 2. *Earth Planet Sci Lett* 293:97–103.
31. Gale AS, Christensen WK (1996) Occurrence of the belemnite *Actinocamax plenus* in the Cenomanian of SE France and its significance. *Bull Geol Soc Den* 43:68–77.
32. Zheng X-Y, et al. (2013) Changing ocean circulation and hydrothermal inputs during Ocean Anoxic Event 2 (Cenomanian-Turonian): Evidence from Nd-isotopes in the European shelf sea. *Earth Planet Sci Lett* 375:338–348.
33. Martin EE, MacLeod KG, Jiménez Berrocoso A, Bourbon E (2012) Water mass circulation on Demerara Rise during the Late Cretaceous based on Nd isotopes. *Earth Planet Sci Lett* 327-328:111–120.
34. MacLeod KG, Martin EE, Blair SW (2008) Nd isotopic excursion across Cretaceous ocean anoxic event 2 (Cenomanian-Turonian) in the tropical North Atlantic. *Geology* 36:811–814.
35. Friedrich O, Erbacher J, Mutterlose J (2006) Paleoenvironmental changes across the Cenomanian/Turonian Boundary Event (Oceanic Anoxic Event 2) as indicated by benthic foraminifera from the Demerara Rise (ODP Leg 207). *Rev Micropaleontol* 49:121–139.
36. Keller G, Berner Z, Adatte T, Stueben D (2004) Cenomanian–Turonian and $\delta^{13}C$, and $\delta^{18}O$, sea level and salinity variations at Pueblo, Colorado. *Palaeogeogr Palaeoclimatol Palaeoecol* 211:19–43.

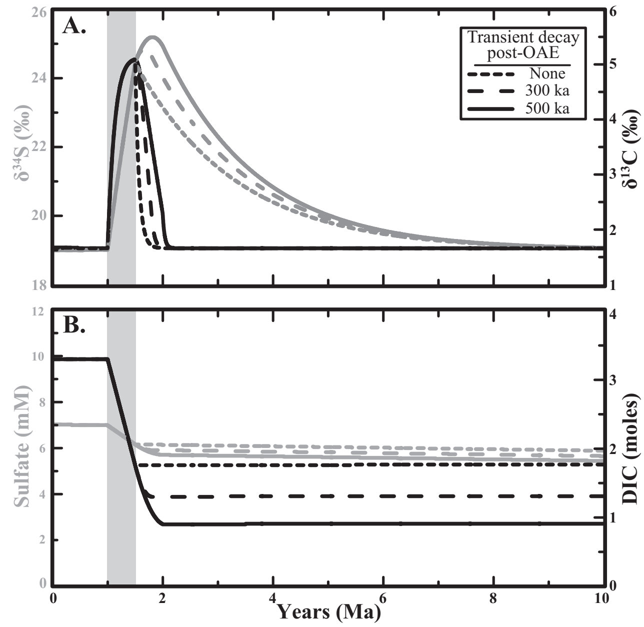

Fig. S1. Sensitivity test for the modeled offset of the coupled carbon and sulfur cycle by varying the amount of time it takes to return to pre-OAE values. This model shows the sensitivity of a waning carbon burial with an increase in the offset of the carbon and sulfur cycles. An increase in time allows for a greater offset and a larger magnitude sulfur-isotope excursion (*A*) whereas having very little effect on the sulfate concentration (*B*). The black lines represent all of the carbon models and blue represents the sulfur models; the dashes for *A* and *B* are shown in the legend of *A*. The models use a twofold increase in pyrite burial, ΔS of −40 during the OAE, and a starting marine concentration of 7 mM.

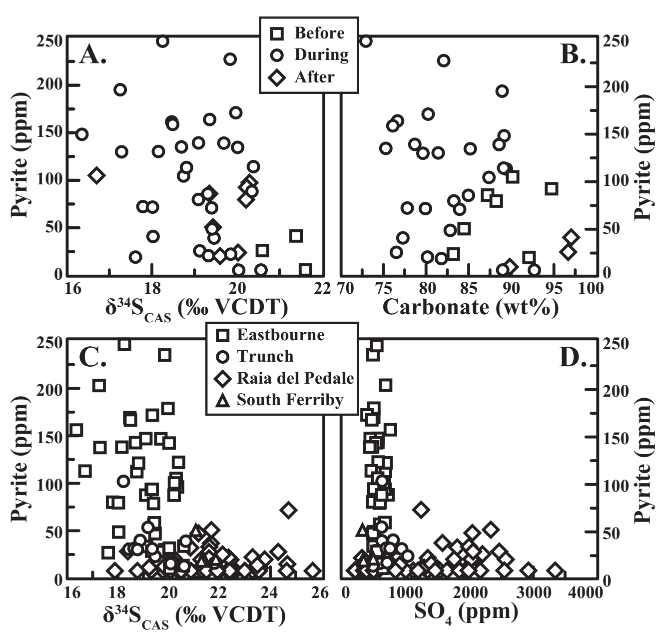

Fig. S2. Cross-plots of geochemical data for Eastbourne (*A* and *B*) and all four sections analyzed in this study (*C* and *D*). In *A* and *B*, pyrite concentrations vs. $\delta^{34}S_{CAS}$ (*A*) and carbonate contents (*B*) show no correlation, indicating that pyrite concentrations have not systematically affected the $\delta^{34}S_{CAS}$ values at Eastbourne. Similarly, *C* and *D* show no correlation for pyrite concentration and $\delta^{34}S_{CAS}$ (*C*) or sulfate concentration (*D*).

Table S1. Initial parameters for the C and S model

Flux (inputs and outputs)	Carbon concentration	$\delta^{13}C$, ‰	Sulfur concentration	$\delta^{34}S$, ‰
Starting marine reservoir	3.3	+1.8	1.35–5.4	+19
Weathering flux	25	−4	0.52* and 0.98†	+5.5
Organic burial	5	−28	—	—
Inorganic burial	20	—	0.67‡ and 0.83§	−11‡ and —§

All fluxes are in 10^{18} mol/Ma, whereas the reservoir sizes are 10^{18} mol. The weathering flux for both cycles combines both the fluxes from volcanic (*) and continental (†) weathering. The isotopic composition of the weathering flux was calculated through isotopic mass balance. The inorganic flux for carbon is based on the burial of carbonates, whereas the sulfur burial portion of the model includes pyrite (‡) and evaporite minerals (§). Em-dashes indicate phases that do not impart a major fractionation on the isotope reservoirs (1), and the $\delta^{34}S$ value for pyrite gives a $\Delta^{34}S$ of −30‰.

1. Kurtz AC, et al. (2003) Early Cenozoic decoupling of the global carbon and sulfur cycles. *Paleoceanography* 18:(4)1090.

Other Supporting Information Files

Dataset S1 (XLS)
Dataset S2 (XLS)
Dataset S3 (XLS)
Dataset S4 (XLS)